INVITED REVIEW

This section of Journal of Materials Research is reserved for papers that are reviews of literature in a given area.

Structure property relationship in $(TiZrNbCu)_{1-x}Ni_x$ metallic glasses

Emil Babić, Damir Pajić, and Krešo Zadro
Department of Physics, Faculty of Science, Zagreb HR-10002, Croatia

Katica Biljaković, Vesna Mikšić Trontl, Petar Pervan, and Damir Starešinić
Institute of Physics, Zagreb HR-10001, Croatia

Ignacio A. Figueroa
Institute for Materials Research-UNAM, Ciudad Universitaria Coyoacan, Ciudad de Mexico C.P. 04510 D.F., Mexico

Ahmed Kuršumović
Department of Materials Science & Metallurgy, University of Cambridge, Cambridge CB3 0FS, U.K.

Štefan Michalik
Diamond Light Source Ltd., Harwell Science and Innovation Campus, DidcotOX11 0DE, U.K.

Andrea Lachová
Institute of Physics, Faculty of Science, P.J. Šafárik University in Košice, Košice 041 54, Slovak Republic

György Remenyi
Institut Neel, Universite Grenoble Alpes, Grenoble F-38042, France

Ramir Ristić[a)]
Department of Physics, University of Osijek, Osijek HR-3100, Croatia

(Received 31 March 2018; accepted 10 May 2018)

The atomic structure, electronic structure, and physical properties of $(TiZrNbCu)_{1-x}Ni_x$ ($x \leq 0.5$) metallic glasses (MGs) were studied in both the high-entropy ($0 < x < 0.35$) and the higher Ni concentration range ($x \geq 0.35$). Atomic structure studies performed with X-ray diffraction and synchrotron powder diffraction provided average atomic volumes, structure factors, radial distribution functions, coordination numbers, and packing densities. Electronic structure studies performed using photoemission spectroscopy and low-temperature specific heat provided information about the electronic density of states within the valence band and at the Fermi level and also about interatomic bonding and atomic vibrations [from the Debye temperature and the boson peak (BP)]. Variations of both atomic structure and electronic structure with x showed a clear change for $x \geq 0.35$, which corresponds to a valence electron number $\geq$7.4. All physical properties, namely, thermal stability parameters, Debye temperatures, BPs, magnetic, elastic, and electronic transport properties, change their concentration-dependence for $x \geq 0.35$. The results are compared with those for binary and ternary MGs of the same elements.

I. INTRODUCTION

"High-entropy alloys" (HEAs) are among the latest and probably the biggest challenge in contemporary condensed matter physics and materials science. HEAs are a new type of alloys based on multiple principal alloying components (four or more) in near equimolar ratios, molar fractions $\leq$0.35.[1–4] This design enables research and probable exploitation of a huge number of completely new systems with structures and properties which can hardly be anticipated.[5,6] Thus, this strategy provides an opportunity to greatly advance our fundamental understanding of the behavior of complex alloys. Moreover, several important problems in physics, including the localization of electrons and phonons, various percolation phenomena on different crystal lattices, and the quantitative distinction between the effects of topological and chemical atomic disorder, can be studied effectively using HEAs. As a result, research on HEAs has led to the preparation of several hundred new alloys, publication of well over a thousand research papers, over ten reviews of the literature (e.g., Refs. 6–15), focus-issues on HEAs in scientific journals, and two books,[16,17] in just over ten years. The majority of these studies deal with their phase(s), microstructure, and mechanical properties, whereas, so far, their physical properties have received relatively little attention, see, for instance, Chapter 7 of Ref. 17, in spite of their potential as functional materials. Especially, puzzling is the near

[a)]Address all correspondence to this author.
e-mail: ramir.ristic@fizika.unios.hr
DOI: 10.1557/jmr.2018.168

absence of experimental studies of the electronic structures of HEAs and of those properties directly related to the electronic structure. In particular, only four studies of their "low-temperature specific heat" (LTSH) have been reported so far[18–21] and the first "angle-resolved photoemission spectroscopy" studies have been performed by us recently.[22] Theoretical studies of the electronic structure of HEAs, although more abundant than experimental ones, are still insufficient and with a few notable exceptions (e.g., Refs. 23–27) are mainly focused on the phases of stability and mechanical properties (see for instance, Chapters 8–11 of Ref. 17). Almost all HEAs studied so far are metallic alloys in which the itinerant electrons provide a large contribution to the cohesive energy, which renders almost all their properties very sensitive to the electronic structure, e.g., Ref. 28 and references therein. So the scarcity of experimental studies of their electronic structures is quite surprising.

The truly multidisciplinary aspect of HEAs, involving researchers from theoretical physics to engineering, has enabled both the breadth and rapid expansion of research on HEAs. Large research efforts in the studies of phases, microstructures, and mechanical properties resulted in a wealth of data confirming the conceptual and technological importance of HEAs.[6–17] In particular, HEAs with ultra-high strength and fracture toughness,[29] outstanding mechanical properties at high temperatures, excellent soft magnetic properties, high fatigue, wear corrosion and irradiation resistance, new biomaterials,[30] and diffusion barriers were recently developed.[14,17] An important feature of HEAs is the simplicity of tuning their properties by adjusting their composition and/or phase content. However, the conceptual understanding of their phases, stability, and properties is still insufficient. In particular, several semi-empirical criteria for the formation of different phases: single phase solid solution, intermetallic compounds, a mixture of intermetallic compounds and solid solutions, and an amorphous phase (a-HEA)[6–17,31] have been used to predict hundreds of solid solution HEAs.[17,32,33] However, so far only a few dozen stable solid solution HEAs have been confirmed by experiment (Chapter 11 of Ref. 17). Part of the problem is that the phases of HEA depend not only on composition but also on preparation and the post-processing conditions. This clearly makes it difficult to judge the success of both semi-empirical and theoretical (e.g., Ref. 14 and Chapters 8–12 of Ref. 17) predictions of phases of HEAs and it also strongly affects their measured properties.

Therefore, in spite of enormous progress made in almost all aspects of research and conceptual understanding, there is still ample space for important contributions to experimental research on the relationship between their electronic structure, atomic structure, and properties, which has been hardly studied so far, and is crucial for deeper conceptual understanding. Furthermore, the studies of HEAs based on the iron group of 3*d*-transition metals (with the addition of Al, Nb, Sn, and metalloids) are by far the most abundant, followed by more recent studies of alloys based on refractory metals, RHEA, and a small number of studies of other alloys such as those containing "rare-earth metals", noble and normal metals, and light elements.[14,17] There are only a few studies of HEAs based on combinations of late 3*d* and refractory/early transition metals in spite of the fact that in such systems, the transitions from a-HEA to simple solid solution HEA, which are conceptually very important, have been reported (e.g., Ref. 18 and Chapter 13 of Ref. 17). Indeed, until recently a-HEAs received relatively little attention[15,18] in spite of the fact that they were the first applications of a new alloy design[1,2] and are of crucial importance for the understanding of some features specific to disorder, such as the boson peak (BP).[18] This was probably due to fact that the prediction of "high-entropy bulk metallic glasses" (HE-BMGs) is probably even more difficult than for conventional binary and multicomponent alloys. Furthermore, the critical thickness of HE-BMGs is generally lower than that of conventional BMGs.[15] More recently, the situation has started to change and several studies showing the conceptual and technological relevance of a-HEAs appeared.[18,34–36]

Our previous[18,36,37] and current work on HEAs is focused on three conceptually important problems in contemporary research on HEAs:

(i) The relationship between the electronic structure, atomic structure, and the intrinsic properties of HEAs.

(ii) The nature and influence of the transition from HEAs to conventional alloys of the same metals, based on one, or at most two, principal alloying components.

(iii) The quantitative disentanglement of the effects of structural/topological and chemical disorder by using the same alloy subjected to different preparation or post-processing treatments.

According to a previous report,[37] the $(TiZrNbCu)_{1-x}Ni_x$ ($x \leq 0.25$) a-HEA system seemed suitable for the study of both problems (1) and (3). Amorphous alloys are suitable for studying (1) because they have a single homogeneous phase and relatively simple electronic structure. In addition, electronic structure and electronic structure–property relations in binary and ternary amorphous alloys of the early (TE) and late (TL) transition metals were found to be particularly simple (e.g., Refs. 28 and 38 and references therein). Furthermore, it was necessary to check whether the HEA design makes some fundamental change to the electronic structure and electronic structure–property relationships or not. Amorphous alloys, especially of the TE–TL type, are also suitable for the study of problem (2), namely, the transition from HEA to conventional alloys in the same alloy system and without a change of the amorphous phase owing to their

broad "glass forming composition range" (GFR). As regards problem (3), it was reported[37] that in these alloys, depending on the preparation method for instance the cooling rate from the melt, either a- or crystalline alloys with a body-centered cubic (bcc) phase can be obtained, which makes them suitable for disentangling the contributions of topological and chemical disorder to their electronic structure and physical properties.

Here, we present the first experimental study to our knowledge of the atomic structure–electronic structure–property relationship in an a-HEA alloy system: $(TiZrNbCu)_{1-x}Ni_x$ ($x \leq 0.5$) for x in both the HEA and Ni-rich ($x \geq 0.35$) concentration range, thus covering problems (1) and (2). Variations of both atomic structure and electronic structure with x show a pronounced change for $x \geq 0.35$ which is reflected in all properties studied, namely thermal stability parameters, Debye temperatures, BPs, magnetic, elastic, and electronic transport properties all show changes in their concentration dependence for $x \geq 0.35$. The results are compared with those for binary and ternary metallic glasses (MGs) of the same elements. We also made numerous attempts to prepare crystalline solid solution HEAs (see Sec. II) with $x = 0.125$ and 0.15, but without success.

II. EXPERIMENTAL

The ingots of seven alloys in the $(TiZrNbCu)_{1-x}Ni_x$ system with $x = 0$, 0.125, 0.15, 0.20, 0.25, 0.35, and 0.5 were prepared from high purity elements (≥99.98%) by arc melting in high purity argon in the presence of a Ti getter. The ingots were flipped and remelted five times to ensure good mixing of components. Ribbons with a thickness of about 20 μm were fabricated by melt spinning molten alloys on the surface of a copper roller rotating at a speed of 25 m/s in a pure He atmosphere [18.36]. Casting with controlled parameters resulted in ribbons with closely similar cross sections ($\sim 2 \times 0.02$ mm^2) and thus for $x \geq 0.125$ with amorphous phases having a similar degree of quenched-in disorder. Molten alloys with $x = 0.125$ and 0.15 were also suction-cast into a water-cooled conical die with a length of 50 mm and base diameter of 8 mm to determine the cooling-rate dependence of the precipitated phase(s) and their contents. (We hoped to find out the conditions for the reported transition from a-HEA to solid solution-HEA with the bcc crystalline structure.[37]) The as-cast samples were investigated by (i) XRD using a Bruker Advance powder diffractometer with a Cu K_α source (Bruker Corporation, Billerica, Massachusetts), (ii) scanning electron microscopy (SEM) using a JEOL ISM7600F microscope with energy-dispersive spectrometry (EDS) capability (JEOL, Ltd., Tokyo, Japan), and (iii) differential thermal analysis (DTA) and differential scanning calorimetry (DSC) using a Thermal Analysis-DSC-TGA instrument (TA Instruments, Inc., New Castle, Delaware). XRD measurements were also performed on crystallized ribbons with $x = 0.125$ and 0.15, in an attempt to verify the reported transition from a-HEA to solid solution-HEA.[37] These ribbons were annealed in a pure argon atmosphere[28] for different times (10–60 min) at several temperatures within the temperature range of the first crystallization maximum[36] in the corresponding DSC traces (773–847 K). The atomic structure of the as-cast samples was also studied using "Synchrotron X-ray powder diffraction" (SXPD) measurements at the I12-JEEP beamline[39] at the Diamond Light Source Ltd., Didcot, United Kingdom. A piece of a sample ribbon was illuminated with a monochromatic beam of 0.1545 Å wavelength and 0.5×0.5 mm^2 size for a total time of 240 s. After every sample measurement, the air scattering signal was measured under the same experimental conditions. X-ray radiation of high energy (80.245 keV) was used to cover high Q values of up to 18 Å^{-1} in reciprocal space, giving information about the atomic pair distribution functions of the as-prepared $(TiZrNbCu)_{1-x}Ni_x$ alloys. All diffraction experiments were carried out in the transmission mode using a flat-panel Pixium RF4343 detector (Thales Group, Vélizy Villacoublay, France). Precise energy calibration was achieved by collecting diffraction data from a fine powder of CeO_2, obtained from NIST, at various standard-to-detector distances. The whole calibration procedure and integration of the two-dimensional X-ray diffraction patterns were performed using DAWN software package.[40]

Thermal measurements were performed with a ramp rate of 20 K/min up to 1550 K. The DTA equipment is regularly calibrated using strontium carbonate and gold standards. This procedure keeps the uncertainty in temperatures derived from DSC-DTA measurements to within ±5 K. The valence-band structure of the as-cast samples was studied with photoemission spectroscopy (PES) performed in an ultra-high vacuum chamber equipped with a Scienta SES100 hemispherical electron analyzer [Scienta Omicron (former VG Scienta), Uppsala, Sweden]. The overall energy resolution in the experiments was 25 meV. An unpolarized photon beam of 21.2 eV was generated by a He-discharge ultraviolet source. The samples were cleaned by several cycles of sputtering with 2 keV Ar^+ ions at room temperature to remove oxygen and other contaminants from the surface. The base pressure during the experiments was below 10^{-9} mbar. Photoemission measurements were also performed on a sample of the alloy with $x = 0.125$ that had been crystallized in situ by holding it at 810 K for 30 min. The as-cast ribbons were also used for measurements of the LTSH, magnetic susceptibility, and mass density D.[18] LTSH measurements were performed in the temperature range 1.8–300 K using a physical property measurement system, Model 6000 from Quantum Design Inc. (San Diego, California).[18,41] The magnetic

susceptibility of all the as-cast and some crystallized samples was measured with a Quantum Design magnetometer, MPMS5, in a magnetic field B up to 5.5 T and temperature range 5–300 K.[18,28,36,38] Since the magnetic susceptibility of all the samples showed a very weak dependence on temperature, as is usual in MGs and compounds of TE and TL metals,[18,28,38] in the following analysis, we will use their room temperature values. The Young's modulus, E, calculated from the relationship $E = Dv^2$, where v is the velocity of ultrasonic waves along the ribbon, was measured both on the as-cast ribbons and the same ribbons relaxed for a short time close to the glass transition temperature of a given alloy.[18,36,38]

III. RESULTS AND DISCUSSION

A. Thermophysical parameters and sample characterization

Because of the vast number of HEAs that can be designed from about eighty stable elements,[10,14] searching for conceptually and technologically interesting compositions by trial and error is clearly inadequate. Therefore, as mentioned in Sec. I, several semi-empirical criteria for the formation of different phases: single phase solid solution, intermetallic compounds and a mixture of intermetallic and solid solution phases, and amorphous phase (a-HEA) have been developed.[6–17,31–33] These criteria are based on thermophysical parameters such as the configurational entropy ΔS_{conf}, the mixing ΔH_{mix} or formation enthalpy ΔH_f, the average difference in atomic sizes of the constituents δ (as in the Hume-Rothery and Inoue's rules, see, e.g., Refs. 13 and 18), etc. (see Gao et al.[42] for an excellent, concise discussion of all semi-empirical criteria and corresponding parameters).

For example, the oldest criterion,[31] a two dimensional ΔH_{mix} (or ΔH_f) − δ plot, where δ is the atomic size mismatch, shows how HEAs evolve with increasing δ and decreasing $\Delta H_{mix}/\Delta H_f$ from solid solution HEAs situated in the region with $\delta \leq 6.6\%$ and -15 kJ/mol $\leq \Delta H_{mix} \leq -5$ kJ/mol to intermetallic and a-HEAs at higher δ and lower or similar ΔH_{mix}.[13,42] To predict the crystal structure type of solid solution HEAs, the "valence electron concentration" (VEC) criterion was proposed.[43] According to this criterion, a bcc phase forms for VEC ≤ 6.87, a mixture of bcc and face-centered cubic (fcc) phase forms for 6.87 ≤ VEC < 8, and an fcc phase appears for VEC ≥ 8. The expressions for all these criteria and the definitions of the corresponding parameters can be found in reviews of the literature[6–17,42] as well as in our previous papers.[18,36]

In Fig. 1, we show the variation with concentration x of parameters ΔH_{mix}, δ and ΔS_{conf} of $(TiZrNbCu)_{1-x}Ni_x$ alloys. Here, the HEA region of x is distinguished from the Ni-rich one ($x \geq 0.35$) by a different color. As already noted,[18,36] the values of the parameters ΔH_f (ΔH_{mix}) and

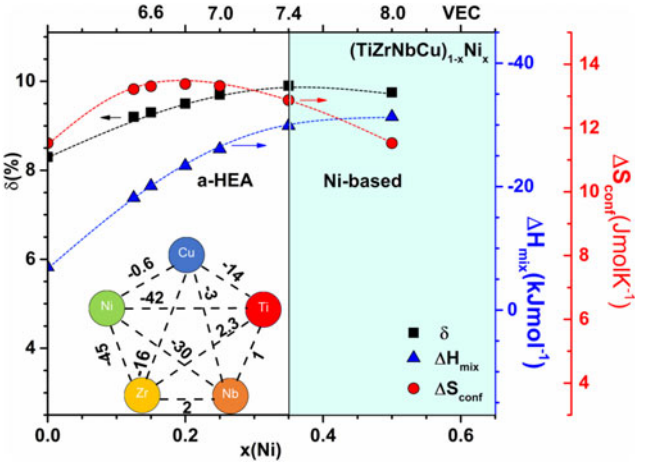

FIG. 1. Thermophysical parameters of $(TiZrNbCu)_{1-x}Ni_x$ alloys versus x and valence electron count, VEC (upper abscissa). Left scale: atomic size mismatch δ, right scale: mixing enthalpy ΔH_{mix} (first right scale), and configurational entropy ΔS_{conf} (second scale). The inset: ΔH_{mix} between constituent elements.[32] Dashed lines are guide for eye.

δ of all alloys are well outside the ΔH_{mix} − δ region in which solid solution HEA forms. (More recent and sophisticated criteria such as those in Refs. 32, 33, and 42 corroborate this conclusion). Regardless of the reliability of ΔH_{mix} − δ[13] and other[32,33] criteria, this conclusion is consistent with our difficulties in trying to convert our alloys with low x to solid solution HEAs. Furthermore, the contribution of the ideal ΔS_{conf} to the free energy is considerably smaller than that of enthalpy[18,36] even at the liquidus temperature T_l so that its effect on phase formation may not be large, as was confirmed by XRD patterns and DSC/DTA results.[18,36] In particular, all melt-spun ribbons with $x > 0$ were fully amorphous, whereas their crystalline counterparts, suction cast rods,[37] and bulk conical samples were multiphase. The inset of Fig. 1 shows that the strong interatomic bonding between TE and TL components, especially between Zr and Ti with Ni, is responsible for the small overall values of ΔH_{mix} (the values of ΔH_{mix} in the inset are taken from Ref. 32). These strong interactions are likely to give rise to "chemical short range order" (CSRO) in the amorphous phase[38] and intermetallic compounds in the crystalline state.[28] Simultaneously, they seem to stabilize amorphous phases since the alloy with $x = 0$ did not vitrify.[18] Similarly, the difference in atomic radii[44] between TE and TL metals is responsible for rather large values of δ which show a maximum at $x = 0.35$.

Since VEC is proportional to x of our alloys, the upper abscissa enables one to follow the variations of the parameters shown in Fig. 1 as a function of VEC. We note that VEC ≤ 7 for $x \leq 0.25$ (HEA region) and reaches 8 for $x = 0.5$ (Ni-rich region). Thus, provided the correlation between VEC and crystal structure of numerous solid solution HEAs[42,43] also applies to TE–TL type

of multicomponent amorphous alloys, the transition from the HEA to Ni-rich concentration range in our alloys could coincide with a change in the "atomic short range order" (SRO), from say bcc-like to mixed bcc–fcc-like and finally to fcc-like. Indeed, an approximate analysis of the first maxima in the XRD patterns of amorphous $(TiZrNbCu)_{1-x}Ni_x$ alloys with $x \leq 0.25$ indicated bcc-like local atomic arrangements,[18] whereas a more recent study of the XRD patterns of the alloys with $x = 0.35$ and 0.5 (Ni-rich concentration region) indicated deviations from the behavior expected for bcc-like atomic arrangements.[36] In particular, the average lattice parameters a calculated from the XRD patterns by assuming bcc-like local atomic arrangements decreased linearly with x for $x \leq 0.25$ (as expected from Vegard's law) but a showed a strong positive deviation for $x \geq 0.35$ (Fig. 2 in Ref. 36). Before discussing in some detail this unusual finding, we will briefly overview the main results of thermal studies and compositional/homogeneity characterization of our samples (given in more detail in Refs. 18 and 36).

The detailed description of SEM/EDS studies performed on our as-cast samples in the HEA composition region, which included SEM images and EDS mapping of the distributions of constituent elements, was given in Ref. 18. Briefly, it was found that the EDS compositions were the same as the nominal ones to within ±1–2 at.% and that the distributions of all constituent elements were random down to the submicrometer scale. We note that suction cast rods of $(TiZrNbCu)_{1-x}Ni_x$ alloys,[37] having nominally the same compositions as our a-HEAs, solidified to form dendritic microstructure and EDS analysis showed that these dendrites, of size 2–5 μm, consisted mainly of Nb. Indeed, quite often the distribution of constituent elements in HEAs is uneven, and this sometimes occurs even in alloys showing solid solution HEA behavior in their XRD patterns.[7] We performed the same type of SEM/EDS study on our samples with higher Ni content ($x \geq 0.35$). These samples also had a random distribution of constituent elements and their EDS compositions agreed well with nominal ones.[36]

The detailed DSC/DTA study of all the samples[36] confirmed the XRD results that the as-cast ribbons with $x \geq 0.125$ were amorphous and provided their glass transition (T_g), crystallization (T_x), melting (T_m), and liquidus (T_l) temperatures. All alloys showed quite complex crystallization behavior with two distinct exothermic maxima for $x \leq 0.25$[36,37] and three maxima in the Ni-rich alloys.[36] For the sake of simplicity, we analyzed only the first crystallization event (allegedly associated with the precipitation of a bcc-HEA phase for $x \leq 0.2$[37]) which determines the stability of the amorphous phase and the width of the supercooled liquid region, $\Delta T_x = T_{x1} - T_g$. Thermal stability parameters T_{x1} and T_l showed qualitatively the same variations with x, a rapid increase for $x \leq 0.25$ and a tendency to saturate in the Ni-rich region (Fig. 4 in Ref. 36). We note that the observed change in concentration dependence of T_x and T_l coincides with that in the average lattice parameters of a bcc-like atomic arrangement (Fig. 2 in Ref. 36). Since T_x and T_l are associated with the strength of interatomic bonding, it seems that a change in SRO at elevated Ni-contents affects the interatomic bonding too. The enthalpies of crystallization ΔH_{c1} and the widths of supercooled liquid region ΔT_x showed similar variations with x as those of T_{x1} and T_l. In particular, ΔT_x increased from about 40 K at low x to about 100 K on the more Ni-rich side. The reduced glass transition temperature T_{rg} (which is frequently employed as a criterion for glass forming ability, e.g., Ref. 28) showed a modest magnitude around 0.52 (thus indicating modest GFA) and rather little variation with x (Fig. 2 in Ref. 36). Since we experienced some difficulties in preparing the fully amorphous alloys with the lowest and the highest Ni-contents and were unable to vitrify the alloy with $x = 0$, the GFA criteria T_{rg} and ΔT_x[28] may not be applicable to present alloys.[36]

B. Atomic structure

As already noted in Sec. III.A, the XRD patterns of amorphous alloys, in addition to showing the amorphous nature of a particular alloy, can also provide some insight into the local atomic arrangements, the average atomic volumes, and the average atomic packing fractions (APFs) (e.g., Refs. 38 and 45). The corresponding procedures were previously[46,47] used by us to correct the $N(E_F)$ of a hypothetical fcc-phase of pure Zr,[48] by providing a better estimate for the corresponding atomic volume, and were also used to determine the atomic volume of amorphous copper and the average APFs of amorphous Cu–Hf alloys.[38] We note that in all these cases, the atomic volumes determined by using XRD patterns agreed quite well with those obtained from the experimental mass-density.[49]

In particular, from the modulus of the scattering vector k_p, corresponding to the first maximum in the XRD pattern,[18,36] $k_p = 4\pi \sin\theta/\lambda$ (θ is the Bragg angle and λ is the wavelength of the X-ray radiation), one can calculate the average nearest neighbor distance[45]:

$$d = \frac{7.73}{k_p} \quad . \tag{1}$$

By assuming an approximate crystal structure of the local atomic arrangement, one can calculate the corresponding average lattice parameter a and the average atomic volume, V. In particular, for a bcc-like local atomic structure, $a_{bcc} = 2d/3^{0.5}$ and $V_{bcc} = a^3/2$, whereas for the fcc-like atomic SRO, $a_{fcc} = 2^{0.5}d$ and $V_{fcc} = a^3/4$. The variation of a_{bcc} of all our alloys with Ni content was shown in Fig. 2 of Ref. 36, whereas a_{bcc} for alloys with $x \leq 0.25$ (VEC ≤ 7) follows Vegard's law for a bcc crystal structure quite well (making allowance for

somewhat lower mass-density of amorphous alloys[36]), the a_{bcc} data for alloys with more Ni (VEC $>$ 7) show a strong upward deviation from the Vegard's law. Here, in Fig. 2, we show the corresponding V_{bcc} values for all our alloys as a function of Ni-content x and VEC (upper abscissa). The variation of V_{bcc} is qualitatively the same as that of a_{bcc},[36] and V_{bcc} tends to "saturate" for $x \geq 0.35$ at values which are considerably larger than those predicted by Vegard's law. The values of V_{fcc}, obtained from XRD patterns by assuming an fcc-like local atomic structure, for $x \geq 0.35$ and also shown in Fig. 2 seem to agree better with the expected, approximately linear, variation of atomic volumes with concentration. This is a rather general feature of metal–metal type amorphous alloys.[38,49,50] Therefore, the variations of both average lattice parameters[36] and atomic volumes with x (Fig. 2) indicate a change in atomic SRO in alloys with more Ni ($x \geq 0.35$, VEC ≥ 7.4).

From the atomic (or molar) volumes, one can also calculate the average local APFs.[50] In particular, the APF for an amorphous alloy, η_a, can be calculated from the expression[50]:

$$\eta_a = \frac{\sum_k \eta_k^0 x_k V_k^0}{V_a} \quad , \qquad (2)$$

where η_k^0 is the APF of the k-th constituent of the alloy in its crystalline state, x_k and V_k^0 are its molar fraction and molar volume in the crystalline state, respectively, and $V_a = M/D$, where M is the molar mass and D is the mass density that was calculated from the atomic volumes of amorphous Ti, Zr, Nb, Cu, and Ni in Ref. 49. As can be seen in the upper part of Fig. 2, these values of η_a are approximately constant, as could be expected because V_a obeys Vegard's law, and fairly high, $\eta_a \approx 0.75 \pm 0.01$. The APF obtained by using V_{bcc} values, (thus V_{bcc} from Fig. 2 instead of V_a) η_{bcc}, is also shown in the upper part of the same figure. η_{bcc} is like η_a approximately constant but is a little lower (lower D[18]) than η_a for $x < 0.25$ but rapidly decreases to $\eta_{bcc} = 0.67$ for $x = 0.5$. Thus, the variations of both V_{bcc} and η_{bcc} indicate changes in atomic SRO for $x \geq 0.35$.

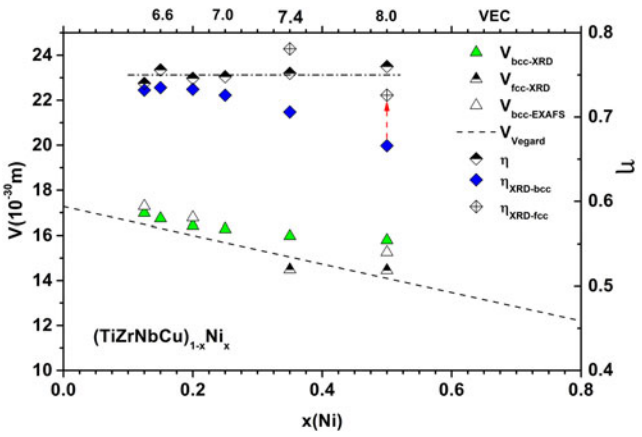

FIG. 2. Atomic volumes and APFs of $(TiZrNbCu)_{1-x}Ni_x$ alloys versus x and VEC (upper abscissa). Left scale: Atomic volume V; right scale: packing fractions η. Dashed lines are guide for eye.

However, by replacing V_{bcc} with V_{fcc} for $x = 0.5$, one recovers the expected approximately constant APF, specific to amorphous alloys of the metal–metal type.[38,50] Thus, the variations of all parameters derived from XRD patterns (Fig. 2 and Ref. 36) indicate a progressive change in local atomic arrangements accompanying the transition from HEA to the concentration region with higher Ni content. This change apparently affects the thermal parameters (Sec. III.A and Ref. 36) and probably the interatomic bonding in the alloys studied.

However, Guinier's procedure[45] for the determination of the average distance between the nearest neighbors in amorphous alloys from XRD patterns has been vigorously criticized (e.g., Ref. 51). Therefore, we recently started SXPD measurements which provide a more direct insight into the possible changes in the atomic SRO, obtained from the structure factors $S(Q)$ and radial distribution functions RDF(r) as well as from a more reliable determination of d. The total X-ray $S(Q)$ was obtained from integrated raw intensity data, $I^{raw}(Q)$, using the procedure described elsewhere.[52,53] Briefly, $I^{raw}(Q)$ was corrected for background (air scattering), self-absorption, fluorescence, and Compton scattering and then scaled and normalized into electron units using the high-angle region method.[54] The corrected intensity, $I^{cor}(Q)$, was used to calculate $S(Q)$ by applying the Faber–Ziman formalism.[55] All the corrections mentioned above were obtained using the PDFGetX2 program.[56]

The $S(Q)$ curves (not shown) consisted of a strong initial peak, followed by a series of broad, damped oscillations extending up to $Q = 16$ Å^{-1}, which together rule out any crystallinity in our samples with $x \geq 0.125$. The position of the first peak shifted rapidly with x to higher Q for $x \leq 0.25$, but the shift slowed down for $x = 0.5$. A more drastic change occurred in the second, split maximum of $S(Q)$ which is probably more directly related to the atomic SRO than the first one (e.g., Ref. 57). In particular, its asymmetry, the difference in the magnitudes of its first and second part (higher Q), was strongly reduced at $x = 0.5$ with respect to those observed for $x \leq 0.25$.

The radial distribution functions RDF(r) were obtained through sine Fourier transformation of $S(Q)$:

$$\mathrm{RDF}(r) = 4\pi r^2 \rho(r) = 4\pi r^2 \rho_0 + r\frac{2}{\pi}\int_0^\infty Q[S(Q)-1]\sin(rQ)\mathrm{d}Q \quad , \qquad (3)$$

where $\rho(r)$ and ρ_0 are the local and average atomic number densities, respectively, and r is the radial distance.

RDF(r) curves shown in Fig. 3 confirm a strong change in both atomic short- and medium-range order occurring for $x = 0.5$. In particular, the shape of the first maximum SRO becomes strongly asymmetric on the right side of the peak, while in the second, split maximum, the magnitude of its second part (higher r) is strongly enhanced with respect to that of its first part. From the positions of the first peaks, we determined corresponding interatomic distances and average bcc-atomic volumes which agree well with those obtained from XRD patterns as demonstrated in Fig. 2. From RDF (r), we also calculated the average coordination number, N (the number of atoms in a spherical shell between radii r_1 and r_2 around an average atom):

$$N = \int_{r_1}^{r_2} \mathrm{RDF}(r)\mathrm{d}r \quad . \tag{4}$$

The variation of N for the cut-off r_2 at the minimum between the first and second maxima in Fig. 3 is shown in the inset of Fig. 3. A strong increase of N is observed at $x = 0.5$, confirming the change in SRO. We note that $N \geq 13$ is usual in multicomponent MGs.[57] Since for high r_2 N may have some contribution from the second atomic shell,[51] we have checked the variations of N for somewhat lower values of r_2 and obtained qualitatively the same variations with x. In particular, for a cut-off at 0.95 r_2, we obtained N increasing from 12.4 for $x \leq 0.25$ to 12.8 at $x = 0.5$. Therefore, the initial results of SXPD provide strong support for a change in atomic arrangements at $x = 0.5$ (VEC = 8). This change is accompanied by an increase in N, which is reminiscent of the proposed correlation between VEC and crystal structure in HEAs.[42,43] Due to the correlation between the local atomic order and electronic structure, we expect strong changes in the electronic structure in the region with more Ni as described in Sec. III.C.

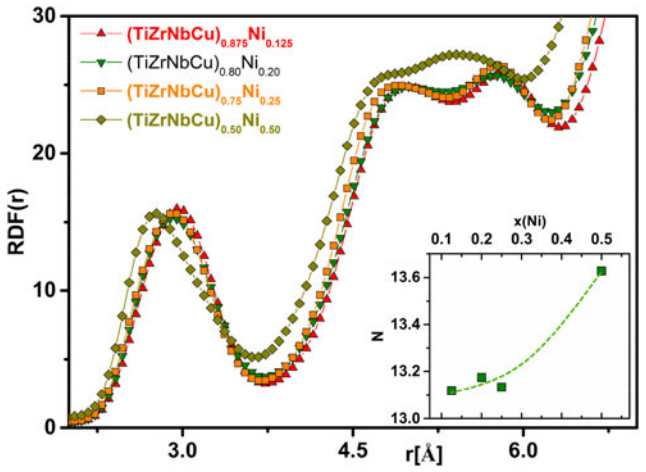

FIG. 3. Radial distribution functions RDF(r) versus r for $(TiZrNbCu)_{1-x}Ni_x$ alloys. The inset: corresponding coordination numbers N versus x. Dashed line in the inset is guide for eye.

C. Electronic structure

As already noted in Sec. I and in several recent papers (e.g., Refs. 18, 25, 28, 36, 38, and 58 for metallic systems, regardless whether they are amorphous or crystalline, the electronic structure controls practically all their intrinsic properties (those that are hardly affected by the exact preparation and/or post-processing conditions). The importance of the electronic structure in understanding the properties of alloys probably shows up the best in the case of amorphous TE–TL alloys. Soon after the discovery of these MGs, the PES revealed the split-band structure of these alloys with TL metals having a full or nearly full d sub-band for which the electronic DoS at the Fermi level, $N_0(E_F)$, is dominated by TE d-states.[59] Thus, the effect of alloying with TL is approximately described by a dilution of a-TE,[60] which simplifies the explanation of the linear variations of most properties of these MGs with TL content.[38,46,60] Furthermore, $N_0(E_F)$ values of TE-rich alloys (determined from LTSH) were higher than those of stable hexagonal close-packed crystalline phases of corresponding TE[61] and were close to those calculated for hypothetical fcc structures of TEs.[48] High $N_0(E_F)$ in TE-rich MGs leads to enhanced superconductivity and magnetic susceptibility[46] but also to weaker interatomic bonding, thus to lower elastic moduli and thermal stability.[62] The combined studies of PES and ab initio calculations were also performed on Zr-based multicomponent MGs and showed that $N_0(E_F)$ is dominated by TE d-electrons as in binary MGs (e.g., Ref. 63). We note that a combination of PES, LTSH, and ab initio theory is the best to fully comprehend the electronic structure. In particular, ordinary PES and LTSH experiments reveal the variation of the total DoS with energy (PES) and give accurate value for $N_0(E_F)$ (LTSH), but they cannot provide accurate contributions of the alloying elements (pDoS) to these quantities. The theory can in principle provide all these quantities as well as the probable local atomic structure (including CSRO[63]) but its results are often limited by the rather small size of the sample and approximations involved in a given calculation (e.g., Refs. 38, 58, and 63).

Accordingly, we performed combined PES[22,64] and LTSH[18,36] studies of a-$(TiZrNbCu)_{1-x}Ni_x$ alloys with x covering both HEA and regions with higher Ni content. The results of PES in the a-HEA region are illustrated in Fig. 4 and compared with those for binary and ternary Zr-based MGs.[65] The recorded "ultraviolet photoemission spectrum" (UPS) reflects the DoS within the valence band of the amorphous $(TiZrNbCu)_{0.8}Ni_{0.2}$ alloy.

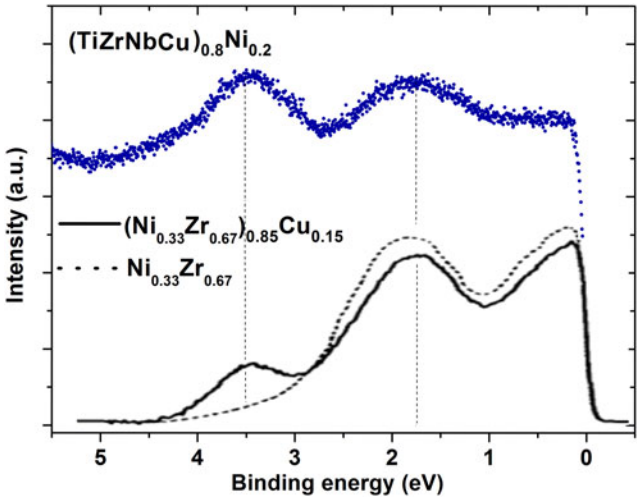

FIG. 4. UPS of $(TiZrNbCu)_{0.8}Ni_{0.2}$ (blue dots[64]), and for comparison, of $(Ni_{0.33}Zr_{0.67})_{0.85}Cu_{0.15}$ and $Ni_{0.33}Zr_{0.67}$ from Ref. 65.

The spectral maximum at 3.5 eV below the Fermi level, associated with the Cu-3*d* states, is well resolved and separated from the low-energy part of the spectrum. From the comparison with the spectrum of amorphous $(Ni_{0.33}Zr_{0.67})_{0.85}Cu_{0.15}$ and $Ni_{0.33}Zr_{0.67}$ alloys,[65] shown in the lower part of Fig. 4, it is evident that the low-energy part of the spectrum has contributions from Ni-3*d* and Zr-4*d* bands.[65] It appears that most of the spectral intensity between 1 and 2 eV below E_F comes from the DoS associated with Ni-3*d* bands.[66,67] The Ni contribution to the intensity at the Fermi level is not negligible and is likely to increase at high Ni-content.[68] The Zr-4*d* band is expected to contribute to the DoS mainly at the Fermi level[69] as is the Ti-3*d* band, as judged from the spectrum from pure Ti[70] and an amorphous $(Ni_{0.33}Zr_{0.67})_{0.85}Ti_{0.15}$ alloy.[65] The Nb-4*d* band contributes to the spectral intensity at the Fermi level and around 1.2 eV[71] but possibly to a lesser extent than Ni.[72] The *s*–*p* bands of all constituents span a larger energy range and generally contribute less to the photoemission intensity. Therefore, we could not extract their contribution to the DoS from the spectra of the alloys. The effects of increasing Ni content x and of crystallization of the sample with $x = 0.125$ on photoemission spectra have also been studied.[64] The present results add to mounting evidence that PES is an efficient tool for assessing the contributions of individual constituents to the electronic properties of 3*d* and 4*d* transition metal-based HEAs. Indeed, the insight obtained from PES will be helpful for the interpretation of LTSH, magnetic susceptibility, and superconductivity data for the same alloys.

As noted above, LTSH provides a quantitative insight into the DoS at E_F which controls the physical properties of metallic systems. In particular, the Sommerfeld coefficient of the linear term in LTSH is given as[18,36,38]

$$\gamma = \frac{\pi^2 k_B^2 N_0(E_F)\left(1+\lambda_{e-p}\right)}{3} \quad , \qquad (5)$$

where k_B is the Boltzmann constant and λ_{e-p} represents the electron–phonon enhancement of the DoS at E_F, $N_0(E_F)$. Since the local atomic arrangements determine the ES of alloys (e.g., Ref. 28), we expect a change of $N_0(E_F)$, thus also γ of our alloys, in going from a-HEAs ($x \leq 0.25$) to conventional amorphous alloys with higher Ni content ($x \geq 0.35$). In Fig. 5, we compare the variations of γ with TL content in our alloys[36] with those in several binary and ternary a-TE–TL alloys composed from the same TEs and TLs.[73–77] In Fig. 5, we plot γ versus total TL content (that of Cu and Ni) in our alloys since in binary TE–TL amorphous alloys, the variations of γ in the alloys with TL = Cu and Ni are very similar, thus it is the total TL content which causes a decrease of γ in alloys containing both Cu and Ni. (If we plotted γ versus Ni content only, as was done in Ref. 36, this will only shift the data in Fig. 5 toward the left but will not change the overall variation with x.) As can be seen in Fig. 5, in our alloys, γ values initially decrease with x as in other a-TE–TL alloys, but they saturate for $x \geq 0.35$, this does not occur in binary alloys at similar TL contents. In particular, γ of binary alloys seems to follow a linear decrease with x throughout the x-range explored ($x \leq 0.70$). Possible exceptions are a-Zr–Ni alloys, which seem to show slower variation of γ with x for $x > 0.60$ (VEC > 7.5).[61] In these alloys, this change is associated with a strong CSRO effect[38,49,61,63] and the change in the position of E_F with respect to the two sub-bands in the DoS, as evidenced by Hall effect and thermopower measurements.[78] Ab initio studies of the atomic and electronic structure of binary amorphous alloys of Ni with Ti, Zr, V, or Nb performed by Hausleitner and Hafner[63] corroborated these findings. They found an increase in CSRO and a change in local atomic order at high Ni contents. Simultaneously, the *d*-band of Ni broadened and shifted towards the Fermi energy. These effects could also affect the variation of γ with Ni content in our alloys, but preliminary measurements of the Hall effect in a-HEAs do not seem to indicate such band-crossing[79] for $x < 0.5$. As regards its magnitude, γ of our alloys with $x = 0.35$ agrees rather better with those for a-Zr–Cu, Ni alloys than with those for a-Ti–Cu, Ni alloys, in spite of the sizable Ti-content. This may be due to the Nb content in our alloys which reduces both their Zr and Ti contents and, as can be seen in Fig. 5, the addition of Nb strongly suppresses γ in a-Zr–Nb–Ni alloys.[77] Since γ depends on the DoS which is enhanced by the electron–phonon interaction, it cannot be used to prove that the change in γ for $x \geq 0.35$ is due to $N_0(E_F)$. However, in superconducting transition metal alloys, one can use the McMillan expression[80] to

disentangle $N_0(E_F)$ from λ_{e-p}. By using the results of recent measurements of the superconducting transition temperatures, T_c,[79] we have calculated the values of $N_0(E_F)$ shown in Fig. 6, which confirm a change in $N_0(E_F)$ for $x \geq 0.35$. Thus, our study of the electronic structure is consistent with that of the atomic structure in Sec. III.B, in that a change of electronic structure accompanies the change in local atomic arrangements for $x > 0.35$. This change in electronic structure exerts strong influence on physical properties, as demonstrated in Sec. III.D.

D. Physical properties

Among the physical properties, the paramagnetic Pauli susceptibility of nonmagnetic alloys is directly related to the electronic structure. However, the magnetic susceptibility χ_{exp} of transition metals and alloys is quite complex and consists of three main contributions[38,48]:

$$\chi_{exp} = \chi_p + \chi_{dia} + \chi_{orb} \quad , \qquad (6)$$

where χ_p is the Pauli paramagnetic contribution of *d*-electrons and χ_{dia} and χ_{orb} are the diamagnetic and orbital paramagnetic contributions, respectively. χ_{dia} and χ_{orb} are calculated by adding corresponding contributions from the constituents.[48,81,82] The Pauli paramagnetism of a *d*-band is enhanced over the free-electron value, $\chi_p^0 = \mu_0\mu_B^2 N_0(E_F)$ (where μ_0 is the permeability of the vacuum and μ_B is the Bohr magneton), by the exchange interaction, namely, $\chi_p = S\chi_p^0$, where S is the Stoner enhancement factor, which also depends on $N_0(E_F)$. But in many amorphous TE–TL alloys,[38] S is nearly constant within their GFR, thus the variation of χ_p with concentration is dominated with $N_0(E_F)$. In spite of its complex structure, χ_{exp} in a-TE–TL alloys often varies with composition in qualitatively the same way as γ.[38] This is probably due to an approximately linear decrease of χ_{orb} with TL content, which does not affect the overall dependence on composition. This has also been observed in our alloys,[36] therefore it seems to be quite general feature of nonmagnetic a-TE–TL alloys which does not depend on their number of components. Indeed, when the variation of χ_{exp} with x of our alloys is compared with those for binary amorphous alloys made of the same constituent TE and TL metals,[22] the result is qualitatively the same as that for the corresponding values of γ shown in Fig. 5. In particular, the variation of χ_{exp} with x for $x \leq 0.35$ is close to that for a-Zr–Ni alloys but tends to saturate for $x > 0.35$ (as does γ in Fig. 5). In Fig. 6, we show that the variations of $\chi_p = \chi_{exp} - (\chi_{dia} + \chi_{orb})$ and $N_0(E_F)$ in our alloys are qualitatively the same, which shows that the change in the electronic structure for $x \geq 0.35$ (VEC = 7.4) affects the magnetic properties of our alloys.

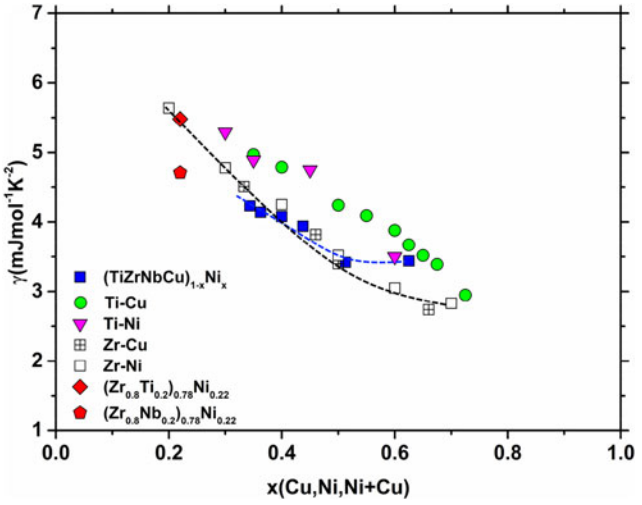

FIG. 5. Variation of electronic coefficient γ versus x for $(TiZrNbCu)_{1-x}Ni_x$[36] and some binary and ternary amorphous alloys. Data for Ti–Cu are from Ref. 73, for Ti–Ni from Ref. 74, for Zr–Cu from Ref. 75, for Zr–Ni from Ref. 76, for $(Zr_{0.8}Ti_{0.2})_{0.78}Ni_{0.22}$ and $(Zr_{0.8}Nb_{0.2})_{0.78}Ni_{0.22}$ from Ref. 77. Dashed lines are guide for eye.

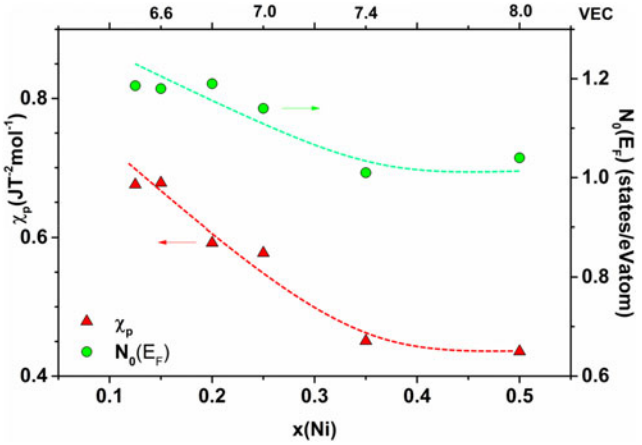

FIG. 6. Density of states $N_0(E_F)$ and Pauli susceptibility for $(TiZrNbCu)_{1-x}Ni_x$ alloys versus x and VEC (upper abscissa). Left scale: χ_p and right scale: $N_0(E_F)$. Dashed lines are guide for eye.

As already noted, LTSH also provides information on the atomic vibrations and interatomic bonding.[18,38,41] This information is contained in the Debye βT^3 phonon term in C_p. Since $\beta \propto \theta_D^{-3}$,[41] one can calculate θ_D from the measured β. The variation of θ_D with x in our alloys shown in Fig. 7 is qualitatively the same as those of the thermal stability parameters T_x and T_l[36]: θ_D increases rapidly for $x \leq 0.35$ but tends to saturate in the Ni-rich region. Since the average atomic mass in the alloys studied changes linearly and relatively little with x,[18] the abrupt change in the variation of θ_D for $x > 0.35$ is apparently related to a change in interatomic bonding and electronic structure, as was the case with T_x and T_l.[36] Careful measurements[18] have shown that C_p increases faster with temperature than the T^3 law predicted by the Debye model.[41] This indicates the presence of the

so-called "BP", an excess of low-energy vibrational states with respect to that predicted by the Debye model (e.g., Ref. 83). A preliminary analysis shows a nonmonotonic variation of the magnitude of BP with Ni-content (the inset of Fig. 7) similar to that of θ_D. To our knowledge, this is the first observation of a possible correlation between the ordinary (θ_D) and excess atomic vibrations in amorphous solids. At present, we have no proper explanation for the observed behavior of the BP in our alloys. However, a change in local atomic arrangements with Ni concentration is expected to affect the atomic vibrations, thus the observed variations of both the BP and θ_D seem plausible. At present, there is no commonly accepted explanation of the BP in glassy systems: some researchers emphasize localized phonon modes (like those caused by oscillations of loosely bonded atoms within the cages of surrounding atoms), whereas others ascribe the BP to a smeared van Hove anomaly.[41,83,84] We note however that the size of the BP depends quite strongly on the amount of the quenched-in disorder which complicates the study of its variation with composition.[84] It is important to note that in our[18,36] and other a-TE–TL alloys (e.g., Ref. 38) as well as in the crystalline cubic TE-based HEAs,[21] the rule-of-mixtures does not describe θ_D properly. This conclusion holds even in the case of a self-consistent choice of the values of θ_D of the constituent elements.[18]

As noted earlier,[18,36,38,46,63,83,85] there is a very simple experimental relationship between ES and mechanical properties (including hardness) and thermal stability (represented by T_x and T_l) of the nonmagnetic a-TE–TL alloys. In particular, a decrease in $N_0(E_F)$ or γ or χ_{exp} is usually accompanied by increases in Young's modulus, hardness, Debye temperature, and thermal stability of these alloys. Therefore, a decrease in DoS at E_F reflects in these systems an increase in the interatomic bonding, and accordingly the stiffness and parameters related to atomic vibrations and thermal stability increase too. We note that such a simple relationship between the electronic structure and interatomic bonding is quite common in crystalline alloys and in nonmagnetic a-TE–TL alloys, it probably stems from their simple electronic band structure.[62] In Fig. 8, we compare the variations of E of our relaxed samples that have received a short anneal close to T_g, with total (Cu + Ni) content to those of binary a-TE–TL alloys composed from the same TEs and TLs.[86–90] Comparing the data in Figs. 5, 6, and 8, we see that a correlation between the electronic structure and E is obeyed by our alloys, too. Furthermore, the approximately linear variation of E with x in binary alloys seems to be replaced by a more complex variation in our multicomponent alloys. This probably reflects a change in the SRO and the electronic structure for x (Cu + Ni) > 0.51. The sensitivity of E to quenched-in disorder and the degree of relaxation introduces considerable uncertainty in the variation of E with x. As already noted,[18,36,38] RoM provides a poor description of E in all a-TE–TL alloys and it also fails to describe the mechanical properties of cubic crystalline TE-based HEAs.[91]

For the sake of completeness, in what follows we briefly summarize some results of an ongoing study of the electronic transport properties of our alloys.[79] As is usual in a-TE–TL alloys,[38] the electrical resistivities ρ of a-$(TiZrNbCu)_{1-x}Ni_x$ alloys are high (>150 μΩ cm) and accordingly decrease with increasing temperature over most of the explored temperature range ($T \leq 300$ K). The variation of their electrical conductivities seems dominated by weak electron localization effects[92] over a broad temperature range (10–300 K) as is usual in a-TE–TL alloys.[93–95] All the samples are superconducting, but with

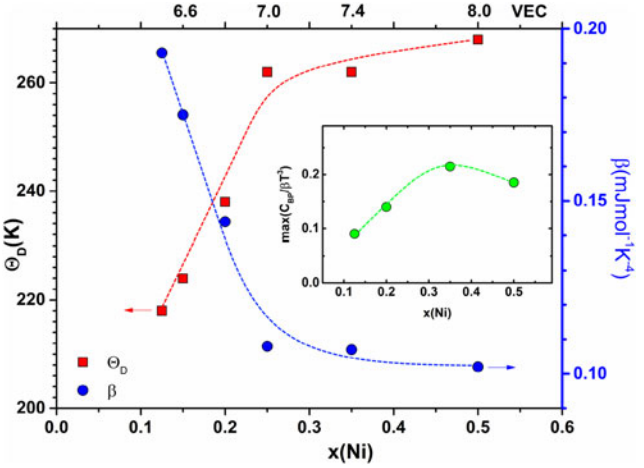

FIG. 7. Phonon coefficients ß and Debye temperatures of $(TiZrNbCu)_{1-x}Ni_x$ alloys versus x and VEC (upper abscissa). Left scale: variation of θ_D; right scale: variation of β. The inset: variation of the magnitude of BP versus x. Dashed lines are guide for eye.

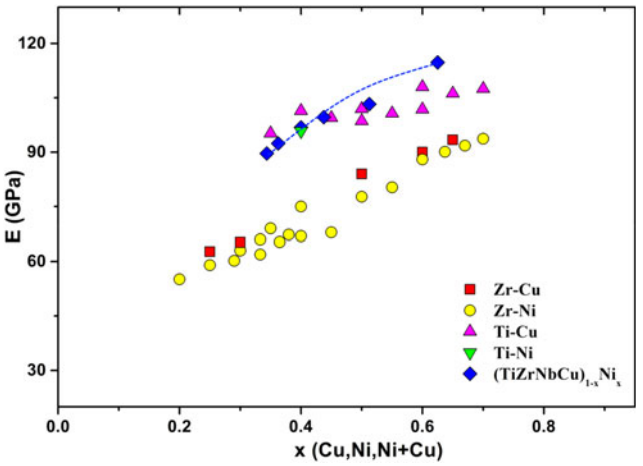

FIG. 8. Variation of E versus x for $(TiZrNbCu)_{1-x}Ni_x$ and some binary amorphous alloys. Data for Zr–Cu are from Refs. 86 and 87, for Zr–Ni from Refs. 86 and 88, for Ti–Cu from Refs. 85, 89, and 90, and Ti–Ni from Ref. 87. Dashed lines are guide for eye.

a low $T_c \leq 1.6$ K. For $x \leq 0.35$, T_c decreases approximately linearly with x, as is usual in nonmagnetic a-TE–TL alloys.[96] However, at higher $x = 0.5$, T_c tends to become constant, hence it follows the same trend with x as γ and $N_0(E_F)$, as is usual for disordered transition metal alloys.[96] A preliminary study of the Hall effect for $x \leq 0.25$ shows that the Hall coefficients R_H are positive and change only a little with x, again in accord with the results for a-TE–TL alloys with lower TL contents.[38,78] Thus, the results for all physical properties of our multicomponent alloys studied until now seem similar to those of the corresponding binary alloys. This probably stems from their similar split-band electronic structures (Fig. 3).

IV. CONCLUSION

The main results of comprehensive experimental studies of the relationship between the atomic structure, electronic structure, and selected physical properties performed on well-characterized multicomponent $(TiZrNbCu)_{1-x}Ni_x$ ($x \leq 0.5$) amorphous alloys are presented. Owing to the broad concentration range explored, the relationship could be studied both in the high-entropy (a-HEA) region ($x \leq 0.25$) and in the region of conventional, Ni-based multicomponent amorphous alloys ($x \geq 0.35$). Such studies are important since the atomic structure and the corresponding electronic structure in metallic systems determine almost all their properties. Therefore, such studies provide a deeper understanding of the properties of the system investigated and moreover enable the prediction of some properties prior to measurement. We note that theoretical, ab initio studies of the atomic structure–electronic structure–property relationship in multicomponent alloys are especially important and will greatly accelerate both the development and understanding of novel complex alloys. However, ab initio studies of novel systems are complementary to experimental studies and cannot fully replace them in the development of novel materials.

The main result of our research is the complete consistency between studies of the atomic structure, electronic structure, and selected physical properties. This clearly demonstrates the power of such an approach because none of the correlations found can be properly described by using the rule-of-mixtures.[18,36]

As regards to the atomic structures, both the results of ordinary X-ray scattering and those from the ongoing study using synchrotron radiation provide evidence that the transition from the HEA composition range to that of conventional Ni-based amorphous alloys for $x \geq 0.35$ and an average number of valence electrons VEC ≥ 7.4 is accompanied by a change in the interatomic arrangements. A possible cause of this change is the strong bonding tendency between Ni and Zr, Ti, or Nb, as shown by the large negative values of H_{mix} in Fig. 1. This results in the development of strong chemical short-range order which is reflected in the electronic structure.[63] The change results in an increase in the number of nearest neighbor atoms (obtained from the radial distribution function) and is therefore consistent with the change from the bcc- to fcc-like local atomic arrangements. A similar type of a change of the crystal structure has been observed previously in crystalline HEAs for VEC ≥ 7.[42,43]

The electronic structure, studied by the "LTSH" and, for the first time, PES, also changes during the transition from the HEA to the conventional alloy region. In particular, the decrease of the electronic density of states at the Fermi level, $N_0(E_F)$ stops for $x \geq 0.35$. A possible cause is the change in the electronic states at the Fermi level from the dominant d-states of Zr and Ti to those of Ni, but further studies, including those of Hall effect and thermopower, are required to prove this conjecture.

As could be expected in metallic systems, the selected physical properties reflect the electronic structure of our alloys. In particular, the decrease of magnetic susceptibility, like that of $N_0(E_F)$, stops for $x \geq 0.35$. This also shows that the correlation between the electronic structure and selected physical properties in the amorphous alloys composed of TE and TL metals does not depend on the number of components of the alloy. The changes in the variations of the vibrational, elastic, and thermal stability parameters with concentration for $x \geq 0.35$ show that a change in the interatomic arrangements is accompanied by a change in the interatomic bonding. In particular, the increase of all these parameters with x stops, or slows down, for $x \geq 0.35$. This is consistent with the conjectured change from bcc- to fcc-like local atomic arrangements.

Finally, we briefly address the relation between the present results for amorphous multicomponent alloys of TE and TL metals with the corresponding results for binary amorphous alloys of Zr and Ti with Cu and Ni. As shown in Sec. III.C and III.D, due to the qualitatively similar split-band structure of the valence bands, both types of alloys show an approximately linear variation of a number of properties related to atomic and electronic structures, over a broad concentration range.[38] However, for binary systems with Cu, this linear variation is preserved over the entire glass forming range ($x \leq 0.9$), in binary alloys with Ni, the linear variation extends up to $x \geq 0.65$ (VEC ≥ 7.9) while for our alloys, it extends up to VEC $= 7.4$. The search for the origin of this difference is in progress.

ACKNOWLEDGMENTS

We thank Professor J.R. Cooper for useful suggestions and Professors E. Tafra and M. Basletić and Mr. M. Kuveždić for sharing their results prior to publication.

Our research was supported by the project IZIP2016 of the University of Osijek. I.A. Figueroa acknowledges the financial support of UNAM-DGPA_PAPIIT, Project No. IN101016. We thank the Diamond Light Source for access to beamline I12 that contributed to the results presented here. A. Lachova acknowledges financial support of the grant VEGA 1/0036/16.

REFERENCES

1. L. Ma, L. Wang, T. Zhang, and A. Inoue: Bulk glas formation of Ti–Zr–Hf–Cu–M (M = Fe–Co–Ni) alloys. *Metall. Trans.* **43**, 277 (2002).
2. B. Cantor, K.B. Kim, and P.J. Warren: Novel multicomponent amorphous alloys. *Mater. Sci. Forum* **386–388**, 27 (2002).
3. J.W. Yeh, S.K. Chen, S.J. Lin, J.Y. Gan, T.S. Chin, T.T. Shun, C.H. Tsau, and S.Y. Chang: Nanostructured high-entropy alloys with multiple principal elements: Novel alloy design concepts and outcomes. *Adv. Eng. Mater.* **6**, 299 (2004).
4. B. Cantor, I.T.H. Chang, P. Knight, and A.J.B. Vincent: Microstructural development in equiatomic multicomponent alloys. *Mater. Sci. Eng., A* **375–377**, 213 (2004).
5. O.N. Senkov, J.D. Miller, D.B. Miracle, and C. Woodward: Accelerated exploration of multi-principal element alloys with solid solution phases. *Nat. Commun.* **6**, 6529 (2015).
6. D.B. Miracle: Critical assessment 14: High entropy alloys and their development as structural materials. *Mater. Sci. Technol.* **31**, 1142 (2015).
7. E.J. Pickering and N.G. Jones: High-entropy alloys: A critical assessment of their founding principles and future prospects. *Int. Mater. Rev.* **61**, 183 (2016).
8. J.W. Yeh: Physical metallurgy of high-entropy alloys. *JOM* **67**, 2254 (2015).
9. M.H. Tsai: Physical properties of high entropy alloys. *Entropy* **15**, 5338 (2013).
10. B. Cantor: Multicomponent and high entropy alloys. *Entropy* **16**, 4749 (2014).
11. Y.F. Ye, Q. Wang, J. Lu, C.T. Liu, and Y. Yang: High-entropy alloy: Challenges and prospects. *Mater. Today* **19**, 349 (2016).
12. Y. Zhang, T.T. Zuo, Z. Tang, M. Gao, K.A. Dahmen, P.K. Liaw, and Z.P. Lu: Microstructures and properties of high-entropy alloys. *Prog. Mater. Sci.* **61**, 1 (2014).
13. S. Guo: Phase selection rules for cast high entropy alloys: An overview. *Mater. Sci. Technol.* **31**, 1223 (2015).
14. D.B. Miracle and O.N. Senkov: A critical review of high entropy alloys and related concepts. *Acta Mater.* **122**, 448 (2017).
15. W.H. Wang: Phase selection in high-entropy alloys: From non-equilibrium to equilibrium. *JOM* **66**, 1 (2014); and references therein.
16. B.S. Murty, J.W. Jeh, and S. Ranganathan: *High-entropy Alloys* (Butterworth-Heinemann, London, 2014).
17. M.C. Gao, J-W. Yeh, P.K. Liaw, and Y. Zhang, eds.: *High Entropy Alloys* (Springer International Publishing, Cham, Switzerland, 2016).
18. K. Biljaković, G. Remenyi, I.A. Figueroa, R. Ristić, D. Pajić, A. Kuršumović, D. Starešinić, K. Zadro, and E. Babić: Electronic structure and properties of $(TiZrNbCu)_{1-x}Ni_x$ high entropy amorphous alloys. *J. Alloys Compd.* **695**, 2661 (2017).
19. J. Lužnik, P. Koželj, S. Vrtnik, A. Jelen, Z. Jagličić, A. Meden, M. Feuerbacher, and J. Dolinšek: Complex magnetism of Ho–Dy–Y–Gd–Tb hexagonal high-entropy alloy. *Phys. Rev. B* **92**, 224201 (2015).
20. S. Vrtnik, P. Koželj, A. Meden, S. Maiti, W. Steurer, M. Feuerbacher, and J. Dolinšek: Superconductivity in thermally annealed Ta–Nb–Hf–Zr–Ti high-entropy alloys. *J. Alloys Compd.* **695**, 3530 (2017).
21. P. Koželj, S. Vrtnik, A. Jelen, S. Jazbec, Z. Jagličić, S. Maiti, M. Feuerbacher, W. Steurer, and J. Dolinšek: Discovery of a superconducting high-entropy alloy. *Phys. Rev. Lett.* **113**, 107001 (2014).
22. E. Babić, K. Biljaković, I.A. Figueroa, A. Kuršumović, V. Mikšić Trontl, D. Pajić, P. Pervan, G. Remenyi, R. Ristić, and D. Starešinić: High-Entropy Alloys: New Challenge in Materials Science. Invited Talk, Solid-State Science & Research Conference, Ruđer Bošković Institute, Scires Book of Abstracts (Zagreb, Croatia, 2017); p. 25.
23. Y. Zhang, G.M. Stocks, K. Jin, C. Lu, H. Bei, B.C. Sales, L. Wang, L.K. Béland, R.E. Stoller, G.D. Samolyuk, M. Caro, A. Caro, and W.J. Weber: Influence of chemical disorder on energy dissipation and defect evolution in concentrated solid solution alloys. *Nat. Commun.* **6**, 8736 (2015).
24. T. Zuo, M.C. Gao, L. Ouyang, X. Yang, Y. Cheng, R. Feng, S. Chen, P.K. Liaw, J.A. Hawk, and Y. Zhang: Tailoring magnetic behavior of CoFeMnNiX (X = Al, Cr, Ga, and Sn) high entropy alloys by metal doping. *Acta Mater.* **130**, 10 (2017).
25. Z. Wu, M.C. Troparevsky, Y.F. Gao, J.R. Morris, G.M. Stocks, and H. Bei: Phase stability, physical properties and strengthening mechanisms of concentrated solid solution alloys. *Curr. Opin. Solid State Mater. Sci.* **21**, 267 (2017).
26. S. Huang, E. Holmström, O. Eriksson, and L. Vitos: Mapping the magnetic transition temperatures for medium- and high-entropy alloys. *Intermetallics* **95**, 80 (2018).
27. M.C. Gao, P. Gao, J.A. Hawk, L. Ouyang, D.E. Alman, and M. Widom: Computational modeling of high-entropy alloys: Structures, thermodynamics and elasticity. *J. Mater. Res.* **32**, 3627 (2017).
28. R. Ristić, K. Zadro, D. Pajić, I.A. Figueroa, and E. Babić: On the origin of bulk glass forming ability in Cu–Hf, Zr alloys. *EPL* **114**, 17006 (2016); and reference therein; E. Babić, R. Ristić, I. Figueroa, D. Pajić, Ž. Skoko, and K. Zadro: Electronic structure and glass forming ability in early and late transition metal alloys. *Philos. Mag.* **98**, 693 (2018).
29. B. Gludovatz, A. Hohenwarter, D. Catoor, E.H. Chang, E.P. George, and R.O. Ritchie: A fracture-resistant high-entropy alloy for cryogenic applications. *Science* **345**, 1153 (2014).
30. M. Todai, T. Nagase, T. Hori, A. Matsugaki, A. Sekita, and T. Nakano: Novel TiNbTaZrMo high-entropy alloys for metallic biomaterials. *Scr. Mater.* **129**, 65 (2017).
31. Y. Zhang, Y.J. Zhou, J.P. Lin, G.L. Chen, and P.K. Liaw: Solid-solution phase formation rules for multi-component alloys. *Adv. Eng. Mater.* **10**, 534 (2008).
32. M.C. Troparevsky, J.R. Morris, P.R.C. Kent, A.R. Lupini, and G.M. Stocks: Criteria for predicting the formation of single-phase high-entropy alloys. *Phys. Rev. X* **5**, 011041 (2015).
33. D.J.M. King, S.C. Middleburgh, A.G. McGregor, and M.B. Cortie: Predicting the formation and stability of single phase high-entropy alloys. *Acta Mater.* **104**, 172 (2016).
34. F. Wang, A. Inoue, F.L. Kong, Y. Han, S.L. Zhu, E. Shalaan, and F. Al-Marouki: Formation, thermal stability and mechanical properties of high entropy (Fe,Co,Ni,Cr,Mo)-B amorphous alloys. *J. Alloys Compd.* **732**, 637 (2018); and references therein.
35. J. Huo, L. Huo, J. Li, H. Men, X. Wang, A. Inoue, C. Chang, J-Q. Wang, and R-W. Li: High-entropy bulk metallic glasses as promising magnetic refrigerants. *J. Appl. Phys.* **117**, 073902 (2015).
36. I.A. Figueroa, R. Ristić, A. Kuršumović, K. Biljaković, D. Starešinić, D. Pajić, G. Remenyi, and E. Babić: Properties of $(TiZrNbCu)_{1-x}Ni_x$ metallic glasses. *J. Alloys Compd.* **745**, 455 (2018).

37. A. Cunliffe, J. Plummer, I. Figueroa, and I. Todd: Glass formation in a high entropy alloy system by design. *Intermetallics* **23**, 204 (2012).
38. R. Ristić, J.R. Cooper, K. Zadro, D. Pajić, J. Ivkov, and E. Babić: Ideal solution behaviour of glassy Cu–Ti, Zr, Hf alloys and properties of amorphous copper. *J. Alloys Compd.* **621**, 136 (2015).
39. M. Drakopoulos, T. Connolley, C. Reinhard, R. Atwood, O. Magdysyuk, N. Vo, M. Hart, L. Connor, B. Humphreys, G. Howell, S. Davies, T. Hill, G. Wilkin, U. Pedersen, A. Foster, N. De Maio, M. Basham, F. Yuan, and K. Wanelik: I12: The joint engineering, environment and processing (JEEP) beamline at diamond light source. *J. Synchrotron Radiat.* **22**, 828 (2015).
40. J. Filik, A.W. Ashton, P.C.Y. Chang, P.A. Chater, S.J. Day, M. Drakopoulos, M.W. Gerring, M.L. Hart, O.V. Magdysyuk, S. Michalik, A. Smith, C.C. Tang, N.J. Terrill, M.T. Wharmby, and H. Wilhelmet: Processing two-dimensional X-ray diffraction and small-angle scattering data in DAWN 2. *J. Appl. Crystallogr.* **50**, 959 (2017).
41. G. Remenyi, K. Biljaković, D. Starešinić, D. Dominko, R. Ristić, E. Babić, I.A. Figueroa, and H.A. Davies: Looking for footprint of bulk metallic glass in electronic and phonon heat capacities of $Cu_{55}Hf_{45-x}Ti_x$ alloys. *Appl. Phys. Lett.* **104**, 171906 (2014).
42. M.C. Gao, C. Zhang, P. Gao, F. Zhang, L.Z. Ouyang, M. Widom, and J.A. Hawk: Thermodynamics of concentrated solid solution alloys. *Curr. Opin. Solid State Mater. Sci.* **21**, 238 (2017).
43. S. Sheikh, H. Mao, and S. Guo: Predicting solid solubility in $CoCrFeNiM_x$ (M = 4d transition metal) high-entropy alloys. *J. Appl. Phys.* **121**, 194903 (2017); and references therein.
44. Available at: https://www.webelements.com.
45. Y. Calvayrac, J.P. Chevalier, M. Harmelin, and A. Quivy: On the stability and structure of Cu–Zr based glasses. *Philos. Mag. B* **48**, 323 (1983).
46. R. Ristić and E. Babić: Thermodynamic properties and atomic structure of amorphous zirconium. *Mater. Sci. Eng., A* **449–451**, 569 (2007).
47. R. Ristić and E. Babić: Magnetic susceptibility and atomic structure of paramagnetic Zr–(Co, Ni, Cu) amorphous alloys. *J. Non-Cryst. Solids* **353**, 3108 (2007).
48. I. Bakonyi, H. Ebert, and A.I. Liechenstein: Electronic structure and magnetic susceptibility of the different structural modifications of Ti, Zr, and Hf metals. *Phys. Rev. B* **48**, 7841 (1993).
49. I. Bakonyi: Atomic volumes and local structure of metallic glasses. *Acta Mater.* **53**, 2509 (2005).
50. D. Ma, A.D. Stoica, and X-L. Wang: Volume conservation in bulk metallic glasses. *Appl. Phys. Lett.* **91**, 021905 (2007).
51. T.C. Hufnagel, R.T. Ott, and J. Almer: Structural aspects of elastic deformation of a metallic glass. *Phys. Rev. B* **73**, 064204 (2006).
52. T. Egami and S. Billinge: *Underneath the Bragg Peaks: Structural Analysis of Complex Materials* (Pergamon Press, Elsevier, Oxford, England, 2003).
53. J. Bednarcik, S. Michalik, V. Kolesar, U. Rutt, and H. Franz: In situ XRD studies of nanocrystallization of Fe-based metallic glass: A comparative study by reciprocal and direct space methods. *Phys. Chem. Chem. Phys.* **15**, 8470 (2013).
54. Y. Waseda: *The Structure of Non-crystalline Materials* (McGraw-Hill Inc., 1980).
55. T.E. Faber and J.M. Ziman: A theory of the electrical properties of liquid metals. *Philos. Mag.* **11**, 153 (1965).
56. X. Qiu, J.W. Thompson, and S.J.L. Billinge: PDFgetX2: A GUI-driven program to obtain the pair distribution function from X-ray powder diffraction data. *J. Appl. Cryst.* **37**, 678 (2004).
57. S. Scudino, M. Stoica, I. Kaban, K.G. Prashanth, G.B.M. Vaughan, and J. Eckert: Length scale-dependent structural relaxation in $Zr_{57.5}Ti_{7.5}Nb_5Cu_{12.5}Ni_{10}Al_{7.5}$ metallic glass. *J. Alloys Compd.* **639**, 465 (2015); N. Mattern, U. Kuhn, H. Hermann, H. Ehrenberg, J. Neufeind, and J. Eckert: Short-range order of $Zr_{62-x}Ti_xAl_{10}Cu_{20}Ni_{10}$ bulk metallic glasses. *Acta. Mater.* **50**, 305 (2002).
58. F. Tian, L.K. Varga, N. Chen, J. Shen, and L. Vitos: Ab initio design of elastically isotropic $TiZrNbMoV_x$ high-entropy alloys. *J. Alloys Compd.* **599**, 19 (2014).
59. P. Oelhafen, E. Hauser, and H-J. Güntherodt: Varying *d*-band splliting in glassy transition metal alloys. *Solid State Commun.* **35**, 1017 (1980).
60. R. Ristić, E. Babić, K. Šaub, and M. Miljak: Electrical and magnetic properties of amorphous $Zr_{100-x}Cu_x$ alloys. *Fizika* **15**, 363 (1983); E. Babić, R. Ristić, M. Miljak, M.G. Scott, and G. Gregan: Superconductivity in zirconium-nickel glasses. *Solid State Commun.* **39**, 139 (1981).
61. I. Bakonyi: Electronic structure and atomic structure of (Ti,Zr, Hf)–(Ni,Cu) metallic glasses. *J. Non-Cryst. Solids* **180**, 131 (1995).
62. R. Ristić, M. Stubičar, and E. Babić: Correlation between mechanical, thermal and electronic properties in Zr–Ni, Cu amorphous alloys. *Philos. Mag.* **87**, 5629 (2007); R. Ristić, E. Babić, M. Stubičar, and A. Kuršumović: Correlation between electronic structure, mechanical properties and stability of TE-TL metallic glasses. *Croat. Chem. Acta* **83**, 33 (2010).
63. M. Hasegawa, H. Sato, T. Takeuchi, K. Soda, and U. Mizutani: Electronic structure of Zr-based metallic glasses. *J. Alloys Compd.* **483**, 638 (2009); C. Hausleitner and J. Hafner: Hybridized nearly free electron tight binding approach to interatomic forces in disordered transition-metal alloys. II. Modeling of metallic glasses. *Phys. Rev. B* **45**, 128 (1992).
64. V. Mikšić Trontl et al.: in preparation, 2018.
65. R. Zehringer, P. Oelhafen, H-J. Güntherodt, Y. Yamada, and U. Mizutani: Electronic structure of $(Ni_{33}Zr_{67})_{85}X_{15}$ (X = Ti, V, Cr, Mn, Fe, Co and Cu metallic glasses studied by photoelectron spectroscopy. *Mater. Sci. Eng.* **99**, 317–320 (1988).
66. V. Mikšić Trontl, P. Pervan, and M. Milun: Growth and electronic properties of ultra-thin Ag films on Ni(111). *Surf. Sci.* **603**, 125–130 (2009).
67. A. Calloni, G. Bussetti, G. Berti, R. Yivlialin, A. Camera, M. Finazzi, L. Duò, and F. Ciccacci: Electronic and magnetic structure of ultra-thin Ni films grown on W(110). *J. Magn. Magn. Mater.* **420**, 356–362 (2016).
68. D. Greig, B.L. Gallagher, M.A. Howson, D.S-L. Law, D. Norman, and F.M. Quinn: Photoemission studies on metallic glasses using synchrotron radiation. *Mater. Sci. Eng.* **99**, 265 (1988).
69. Y. Takahara and N. Narita: Local electronic structures and chemical bonds in Zr-based metallic glasses. *Mater. Trans.* **45**, 1172 (2004).
70. H. Höchst, P. Steiner, G. Reiter, and S. Hiifner: XPS Valence Bands of Ti, Zr, Nb, Mo and Hf. *Z. phys. B: Condens. Matter* **42**, 199 (1981).
71. P. Xiang, J.S. Liu, M.Y. Li, H.F. Yang, Z.T. Liu, C.C. Fan, D.W. Shen, Z. Wang, and Z. Liu: In situ electronic structure study of epitaxial niobium thin films by angle-resolved photoemission spectroscopy. *Chin. Phys. Lett.* **34**, 077402 (2017).
72. J. Kübler, K.H. Bennemann, R. Lapka, F. Rösel, P. Oelhafen, and H-J. Güntherodt: Electronic structure of amorphous transition-metal alloys. *Phys. Rev. B* **23**, 5176 (1981).
73. D.E. Moody and T.K. Ng: Low temperature specific heats of amorphous Cu–Ti alloys. In *LT17 Proceedings*, U. Eckern, A. Schmid, W. Weber, and H. Wühl, eds. (Elsevier Science Publishers B.V, 1984); p. B06.
74. S. Kanemaki, M. Suzuki, Y. Yamada, and U. Mizutani: Low temperature specific heat, magnetic susceptibility and electrical resistivity measurements in Ni–Ti metallic glasses. *J. Phys. F: Met. Phys.* **18**, 105 (1988).

75. P. Garoche and J. Bigot: Comparison between amorphous and crystalline phases of copper–zirconium alloys by specific-heat measurements. *Phys. Rev. B* **28**, 6886 (1983).
76. M. Matsuura and U. Mizutani: Low-temperature specific heat study of $Ni_{100-x}Zr_x$ (x = 30–80) metallic glasses. *J. Phys. F: Met. Phys.* **16**, L183 (1986).
77. M.G. Karkut and R.R. Hake: Upper critical fields and superconducting transition temperatures of some zirconium-base amorphous transition-metals alloys. *Phys. Rev. B* **28**, 1396 (1983).
78. J. Ivkov, E. Babić, and R.L. Jacobs: Hall effect and electronic structure of glassy Zr-3*d* alloys. *J. Phys. F: Met. Phys.* **14**, L53 (1984).
79. M. Kuveždić, E. Tafra, M. Basletić, R. Ristić, V. Mikšić Trontl, P. Pervan, I.A. Figueroa, and E. Babić: Electronic structure and transport properties of $(TiZrNbCu)_{1-x}Ni_x$ metallic glasses. in preparation, 2018.
80. W.L. McMillan: Transition temperature of strong-coupled superconductors. *Phys. Rev.* **167**, 331 (1968).
81. J. Banhart, H. Ebert, and J. Voitlander: Diamagnetic susceptibility of pure metals and binary alloys. *J. Magn. Magn, Mater.* **61**, 221 (1986).
82. C.M. Place and P. Rhodes: Paramagnetic orbital susceptibility of transition metals. *Phys. Status Solidi B* **47**, 475 (1971).
83. Y.Q. Cheng and E. Ma: Atomic-level structure and structure–property relationship in metallic glasses. *Prog. Mater.Sci.* **56**, 379 (2011).
84. A. Salčinović Fetić, G. Remenyi, D. Starešinić, A. Kuršumović, E. Babić, S. Sulejmanović, and K. Biljaković: Analysis of the fragility of the $Zr_{77}Ni_{23}$ metallic glass based on low-temperature heat capacity measurements. *Phys. Rev. B* **96**, 064201 (2017).
85. R. Ristić, E. Babić, M. Stubičar, A. Kuršumović, J.R. Cooper, I.A. Figueroa, H.A. Davies, I. Todd, L.K. Varga, and I. Bakonyi: Simple correlation between mechanical and thermal properties in TE–TL (TE = Ti, Zr, Hf; TL = Ni, Cu) amorphous alloys. *J. Non-Cryst. Solids* **357**, 2949 (2011).
86. Ž. Marohnić, M. Guberović, E. Babić, and G.J. Morgan: Induced conductivity anisotropy in glassy $Zr_{1-x}M_x$ alloys. *J. Phys. F: Met. Phys.* **17**, 1123 (1987).
87. S.H. Whang, D.E. Polk, and B.C. Giessen: Hardness versus Young's modulus of metallic glasses. In *Proceedings of the Fourth International Conference on Rapidly Quenched Metals*, T. Masumoto and K. Suzuku, eds. (Japan Institute of Metals, Sendai, 1982); p. 1365.
88. R.W. Cohrane, J. Destry, M. El Amrani, Z. Altounian, and J.O. Strom-Olsen: Pressure dependence of the resistivity of amorphous NiZr alloys. In *Proceedings of the Fourth International Conference on Rapidly Quenched Metals*, S. Steeb and H. Warlimont, eds. (Elsevier, 1985); p. 1083.
89. L.A. Davis, C-P. Chou, L.E. Tanner, and R. Ray: Strength and stiffnesses of metallic glasses. *Scr. Mater.* **10**, 937 (1976).
90. R. Ristić, E. Babić, D. Pajić, K. Zadro, A. Kuršumović, I.A. Figueroa, H.A. Davies, I. Todd, L.K. Varga, and I. Bakonyi: Properties and atomic structure of amorphous early transition metals. *J. Alloys Compd.* **504S**, S194 (2010).
91. S. Maiti and W. Steurer: Structural-disorder and its effect on mechanical properties in single-phase TaNbHfZr high-entropy alloy. *Acta Mater.* **106**, 87 (2016).
92. H. Fukuyama and K. Hoshino: Effect of spin-orbit interaction on magnetoresistance in the weakly localized region of three-dimensional disordered systems. *J. Phys. Soc. Jpn.* **50**, 2131 (1981).
93. K. Šaub, E. Babić, and R. Ristić: Quantum corrections to conductivity of glassy $Zr_{100-x}Cu_x$ alloys. *Solid State Commun.* **53**, 269 (1985).
94. E. Babić and K. Šaub: Universal conductivity variation in glassy Zr–M alloys. *Solid State Commun.* **56**, 111 (1985).
95. R. Ristić, E. Babić, and K. Šaub: Temperature and concentration dependence of the electrical resistivity of Zr–Cu and Zr–Ni glassy alloys. *Fizika* **21**(Suppl. 1) 216 (1989).
96. E. Tafra, M. Basletić, R. Ristić, E. Babić, and A. Hamzić: Enhanced superconductivity in Hf-base metallic glasses. *J. Phys.: Condens. Matter* **20**, 425215 (2008).